Preprints (www.preprints.org) | NOT PEER-REVIEWED | Posted: 2 January 2020 doi:10.20944/preprints202001.0018.v1

Article

Measurement and Modeling of the 3-D Solar Irradiance for Vehicle-Integrated Photovoltaic

Kenji Araki [1,*], Yasuyuki Ota [2], and Masafumi Yamaguchi [1]

[1] Toyota Technological Institute, Nagoya 468-8511, Japan; masafumi@toyota-ti.ac.jp
[2] Organization for Promotion of Tenure Track, University of Miyazaki, Miyazaki 889-2192, Japan; y-ota@cc.miyazaki-u.ac.jp

* Correspondence: cpvkenjiaraki@toyota-ti.ac.jp; Tel.: +81-52-809-1830

Featured Application: New energy cars.

Abstract: The energy yield of the Vehicle-integrated photovoltaic (VIPV) differs from that of the standard photovoltaics (PV). It is mainly by the difference of the solar irradiance onto the car-roof and car-bodies as well as its curved-shape. Both meaningful and practical modeling and measurement of the solar irradiance for VIPV are needed to be newly established, not the extension of the current technologies. The solar irradiance was modeled by a random distribution of the shading objects and car-orientation with the correction of the curved surface of the PV modules. The measurement of the solar irradiance onto the car-roof and car-body was done using five pyranometers in five local axes on the car for one year. The measured dynamic solar irradiance onto the car-body and car-roof was used for validation of the solar irradiance model in the car.

Keywords: photovoltaic; EV; PHV; standardization; car-roof; flexible PV; performance modeling; rating

1. Introduction

Let us think about a solar-engine car, by the recent development and prevail of EV (Electric vehicle) and PHV (Plug-in hybrid vehicle). The PV technologies will be game-changing in the automobile industry. It may be a dream now, but it is worth challenging [1].

The case study of the photovoltaic (PV) driven cars was conducted both by car manufacturers [2] and a think tank [3], and both reached the same conclusion in 2017. About 70 % of a vehicle can run exclusively by solar energy [2-3]. The calculation base was published, namely: projected area of PV is 3.23 m^2, temperature loss is 9 %, MPPT loss is 5 %, DC-DC converter loss is 10 %, battery charging and discharging loss is 5 %, Electronic Control Unit (ECU) loss is 0.12 kWh/day, mileage is 12.5 km/kWh to Electric Vehicles (EV), 10 km/kWh to Plug-in Hybrid Vehicles (PHV), and the battery size is 40 kWh to EV and 10 kWh to PHV. Then, the requirement of the car-roof PV will be 1 kW. As a result, 70 % of the cars (runs less than 30 km/day) are expected to run by solar energy [2-4]. When we multiply 71 million vehicles (annual sales in 2017), the expected sales will be 50 GW/year [1, 5].

The efficiency and power rating, as well as energy prediction under the curved surface affected by the shading objects, are critical. For example, the car-roof is three-dimensionally curved, and its curvature may induce power loss by increased cosine loss and self-shading loss [1, 6-10]. The irradiance and temperature of the car-roof are different from that of the roof-top or the ground mounting systems [6]. The expected energy yield should be different.

Car roofs are often shaded, resulting in significant losses by the string mismatching [1]. It may be improved by the introduction of a power distribution circuit for compensating the mismatch [6, 11-13]. However, due to the limited area and allowed thickness on the car-roof, the most practical approach is increasing the number of series-connected strings [14].

© 2020 by the author(s). Distributed under a Creative Commons CC BY license.

Preprints (www.preprints.org) | NOT PEER-REVIEWED | Posted: 2 January 2020 doi:10.20944/preprints202001.0018.v1

Another aspect is that the car-roof PV is not in the installation of the standard slope angle and orientation. The orientation of the car-roof changes by time without correlation to the sun direction. Surrounded buildings and other objects (trees and signals) often shade PV panels, and the variety of the curved shape has a complicated impact. Such interaction is needed to take into account [1].

The development of meaningful testing and modeling methods were done by the international group using a web-meeting [6-9]. The 3-D model of photovoltaic power generation developed initially in the car-roof PV, namely VIPV (Vehicle integrated photovoltaic), can be extended to VIPV applications with curved PV using a flexible one.

This article covers the modeling and measurement of the solar-irradiance of the car-body for accurate, meaningful, and non-biased estimation of the energy yield of automobile mounting PV modules.

2. Model

With the progress of the automotive technology, it will help to cover the limited power output of the car-roof PV so that most of the private cars will be able to run by solar energy equipped with high-efficiency and 3-D curved solar panels [1-3], and will overcome the loss mentioned above. To do so, the conventional IEC 60904 international standard series for PV electrical characterization, now focusing on 2-D flat panels, will need to expand to 3-D shaped PV modules [1, 5-10]. We attempt to define 3-D solar irradiation and rating to the 3-D curved solar panels. We also have to consider the cross effect between the 3-D curved surface of the PV module and 3-D solar irradiance around the module [14-16].

The standard PV modules are installed to avoid shadows. However, the car-roof PV is not orientated for the utilization of solar energy. The driver's convenience often shades the PV. The relative orientation of the PV on the car to the sun position is not fixed but frequently changes by driving. The PV on the car body and the car roof are curved. It often shaded by its surfaces. Therefore, the scale of performance is to be reconstructed.

The position and height of the shading objects are often difficult to predict. For predicting the total solar energy to a vehicle (either annual or monthly basis) in a specific area, not in a particular driving course, it is convenient to predict the shading influence using rough indicators of the roughness of the land. The value of the annual or monthly solar irradiance value in a specific area is valuable to predict the driving performance of vehicles mounting the PV panel.

We have to consider the following car-specific issues.

1. More chance of shading by objects around the car (trees and buildings)
2. Curved surface
3. The orientation angle randomly varies.
4. Mismatching loss by partial shading

2.1. Shading probability

The shading influence is complicated and varies by the position and the relative orientation (to the sun position) of the panel. In the case of the car-roof PV, the position (orientation) of the panel cannot be predicted. One practical approach is to rely on the probability model, supposing that some statistical model randomly distributes the distribution of height and density of the shading objects, and the orientation of the car is independent and random as well.

Assuming the segmented annular region, and the building or other shading objects are randomly distributed in this region with random height (Figure 1), the probability of the shading can be approximated as linear relationship [14, 16], because the height of the shading object is assumed to be inversely proportional to the distance from the car, whereas the number of the shading objects along the arc of the given distance is proportional to the distance from the car so that the product of two factors will be the constant value (Figure 2). Note it is convenient to represent the height of the surrounding buildings and other shading objects scaling by the shading angle (grazing angle) [14, 16].

Supposing the height of the shading object (represented by shading angle, namely, grazing angle) is distributed by the ranged uniform distribution, the accumulated distribution as a function of the

Preprints (www.preprints.org) | NOT PEER-REVIEWED | Posted: 2 January 2020 doi:10.20944/preprints202001.0018.v1

shading angle (grazing angle) is calculated as a ranged integral so that the general trend is a linear starting one at zero degrees of the shading angle (grazing angle). It is also important to note that the distribution of the shading objects to the car and building is not axially symmetry and different in the direction to the parallel to the road and orthogonal to the road. Typically, the shading probability of the car-roof PV along the road is less than that of the orthogonal direction of the road in the local coordinate. The area of the segmented annular is convenient to model such a situation (Figure 1) [14, 16]. Note that the annular in place of the disk should be considered to avoid the situation of "division by zero" in angle calculation [14, 16]. Also note that the line slope varies in two directions, one is along the road, and another is orthogonal to the road [14, 16]. A single parameter can represent this trend. Namely, average shading height, corresponding to the 50 % of probability of shading [14, 16].

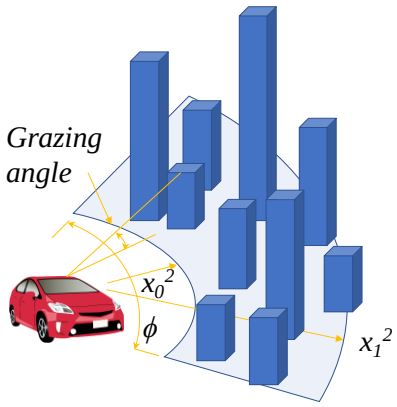

Figure 1. Illustration of the segmented annular region for modeling distribution of the shading objects around the PV panel.

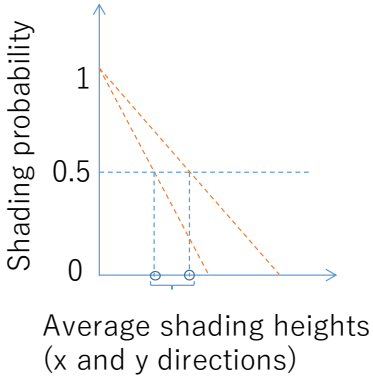

Figure 2. The distribution curve of the shading probability used to the model.

2.2. 3-D irradiance model

For modeling the solar irradiance of the car-roof, we assumed a simple shading and scattering reflection model. The entire shading objects were assumed that the reflectance was 0.25, and reflection is Lambertian. Both direct and scattered solar irradiance were assumed to be shaded by the shading objects as a function of the sun-height and DNI (direct normal irradiance). The probability of the shading event calculated the shading probability and solid angle.

Assuming that the diffused irradiance from the unshaded sky is uniform, the factor of the diffused sunlight relative to the unshaded sky was approximated by the equation (1) using random numbers. Note that the shape of buildings and other shading objects are rectangular, and they are not spherical triangles or spherical trapezoids. It is realistic to model it as a cylinder sky using equation (1).

Preprints (www.preprints.org) | NOT PEER-REVIEWED | Posted: 2 January 2020 doi:10.20944/preprints202001.0018.v1

$$\boldsymbol{\sigma_s}(\theta_h) = 1 - (1 - R_b)\left({}^{\theta_h}/_{90^\circ}\right) \tag{1}$$

where, $\boldsymbol{\sigma_s}(x)$ is a function of the ratio of the diffused sunlight from the sky excluding the reflection of the direct sunlight to the shading objects, R_b is the reflectance of the shading objects (fixed to 0.25 in this calculation), θ_h is the average height of the shading objects scaled by the grazing angle (note that the maximum angle is 45° in this model).

The direct sunlight was approximated by Equation (2).

$$\boldsymbol{\sigma_d}(\eta, \theta_h) = \begin{bmatrix} 0 & (\eta < 0) \\ {}^{\eta}/_{2\theta_h} & (0 \le \eta \le 2\theta_h) \\ 1 & (\eta > 2\theta_h) \end{bmatrix} \tag{2}$$

where, $\boldsymbol{\sigma_d}(x, y)$ is a function of the ratio of illumination of the direct sunlight with the sun height x and the average shading height y.

The scattered sunlight by the reflection of the building from the direct sunlight was approximated by Equation (3) and (4). Note that the scattered irradiation by the reflection of the direct sunlight is seen one-side of the car body (not both sides), and the impact is half of the reflection by scattered light.

$$\boldsymbol{\sigma_{bsh}}(\eta, \theta_h) = \frac{1}{2} R_b \left({}^{\theta_h}/_{90^\circ}\right) \boldsymbol{\sigma_d}(\eta, \theta_h) \cos\eta \tag{3}$$

$$\boldsymbol{\sigma_{bsv}}(\eta, \theta_h) = \frac{1}{4} R_b \left({}^{\theta_h}/_{90^\circ}\right) \boldsymbol{\sigma_d}(\eta, \theta_h) \cos\eta \tag{4}$$

where, $\boldsymbol{\sigma_{bsh}}(x, y)$ and $\boldsymbol{\sigma_{bsv}}(x, y)$ are functions of the ratio of illumination by the scattered reflection from the direct sunlight onto the horizontal and vertical planes with the sun height x and the average shading height y. Note that the illumination by the wall of the building happens on a single side of the road.

For the directional cosine of the direct sunlight to the car-side (vertical plane, random orientation) was approximated by Equation (5).

$$\mathbf{c\theta_{side}}(\omega) = \frac{\int_{0^\circ}^{360^\circ} \cos(\gamma - \alpha(\omega))\left(\cos(\gamma - \alpha(\omega)) > 0\right) d\gamma}{360^\circ} \cos(\eta(\omega)) \tag{5}$$

where, $\mathbf{c\theta_{side}}(\omega)$ is a function of the directional cosine of the direct sunlight to the car-body as a function of the hour angle ω. The sun height η and the azimuth angle α are also the functions of ω. This equation also contains Boolean algebra in the parentheses that returns 1 when the conditional equation is true and 0 when the conditional equation is false. Note that the azimuth angle is not needed to be considered in the calculation on the irradiance on the car-roof (horizontal plane).

The irradiance on the car-roof was approximated using the direct normal irradiance *DNI* and diffused irradiance from the sky *SI* using Equation (6) with calculation results of Equation (1), (2), and (3).

$$CI_{roof} =\cdot \sigma_s \cdot SI + (\sigma_d \sin\eta + \sigma_{bsh}) \cdot DNI \tag{6}$$

where, CI_{roof} is solar irradiance onto the car-roof affected by surrounding shades. Note that the arguments of functions in Equation (6) are omitted.

The irradiance on the car-sides (both the direction parallel to the road and orthogonal to the road) were approximated by Equation (7) using Equation (1), (2), (4), (5) and (6).

$$CI_{side} = \frac{R_r}{2} CI_{roof} + \frac{\sigma_s}{2} \cdot SI + (\sigma_d . c\theta_{side} + \sigma_{bsv}) \cdot DNI \tag{7}$$

where, CI_{side} is solar irradiance onto the car-side affected by surrounding shades, and R_r is a reflection of the road. Note that the arguments of functions in Equation (7) are omitted as well.

Preprints (www.preprints.org) | NOT PEER-REVIEWED | Posted: 2 January 2020 doi:10.20944/preprints202001.0018.v1

2.3. Relation to the conventional solar irradiance model

For a definition of the angle of the solar irradiance and module orientation, the reference axis should be local to the automobile [1]. Each axis moves by the movement of the vehicle, and it is independent of the orientation of the sun. On the other hand, the relative position is unchanged, and thus a linear coordinate conversion dynamically synchronized to the location, direction, and speed of the car, monitored by a GPS, can handle this situation. The coordinate is orthogonal one (Figure 3).

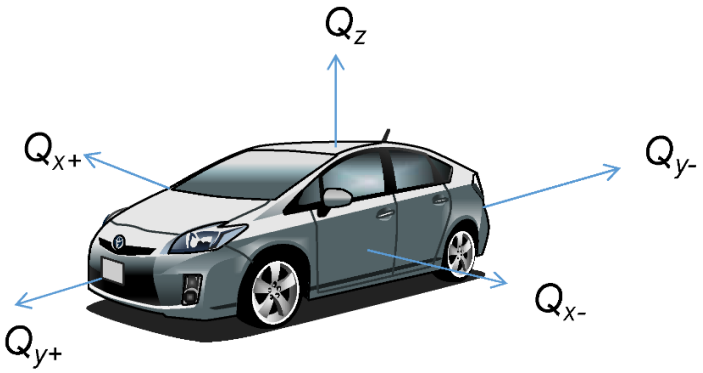

Figure 3. Three-dimensional irradiance around the car-body [1].

Supposing that the orientation of the car is independent of the sun's position and random, the standard and local irradiance parameters of the car-body can be converted to the following nine equations [1]. Some functions and equations contain Boolean algebra, and they return one or zero depending on whether the operation results are true or false. The vehicle body was always assumed level.

$$Q_{roof} = Q_Z \tag{8}$$

$$Q_{side} = \frac{Q_{X+} + Q_{X-} + Q_{Y+} + Q_{Y-}}{4} \tag{9}$$

$$\Phi = \text{if}\left(Q_Z > Q_{th}, \tan^{-1}\left(\frac{\left| \max\left(Q_{X+}, Q_{X-}\right) \right|}{\left| \max\left(Q_{Y+}, Q_{Y-}\right) \right|} \right), NaN \right) \tag{10}$$

$$D = \text{if}\left(\min\left(Q_{X+}, Q_{X-}\right) + \min\left(Q_{Y+}, Q_{Y-}\right) < Q_{side}, Q_Z > Q_{th}, 0 \right) \tag{11}$$

where Q_{roof} is the irradiance onto the car-roof. Q_{side} is the averaged irradiance of the car-sides. Since the orientation of the car is independent of the sun's orientation, the side irradiation may be regarded as the averaged value from four car-sides. Φ is the main angle of the solar beam onto the car-roof. Q_{th} is the threshold of the effective measurement value of the irradiance. It must be greater than zero (non-zero value). *NaN* represents a missing or faulted value. D is the discriminant of the non-shaded condition. False (=0) if the car-roof is shaded. The function **if**(condition, x, y) returns x if condition is true (non-zero), y otherwise. The function **max**(A, B, C, ...) returns the largest value from A, B, C, ... The function **min**(A, B, C, ...) returns the smallest value from A, B, C, ... Note that Equation (10) contains two-dimensional vector calculation, and Equation (11) contains the Boolean algebra.

The orientation angle of the principal solar beam, not always equal to the orientation angle of the direct beam, is calculated by the following equations.

$$Q_{S1} = \max\left(Q_{X+}, Q_{X-}, Q_{Y+}, Q_{Y-}\right) \tag{12}$$

Preprints (www.preprints.org) | NOT PEER-REVIEWED | Posted: 2 January 2020 doi:10.20944/preprints202001.0018.v1

$$Q_{S2} = \max 2\,\mathrm{nd}\left(Q_{X+}, Q_{X-}, Q_{Y+}, Q_{Y-}\right) \tag{13}$$

$$a_{x1} = \left(Q_{S1} = Q_{X+}\right)\frac{\pi}{2} + \left(Q_{S1} = Q_{Y-}\right)\pi + \left(Q_{S1} = Q_{X-}\right)\frac{3\pi}{2} \tag{14}$$

$$a_{x2} = \left(Q_{S2} = Q_{X+}\right)\frac{\pi}{2} + \left(Q_{S2} = Q_{Y-}\right)\pi + \left(Q_{S2} = Q_{X-}\right)\frac{3\pi}{2} \tag{15}$$

$$G = mod\left(\mathrm{if}\left(\left(Q_{S1} > Q_{ths}\right)\left(\left|a_{x1} - a_{x2}\right| = \frac{\pi}{2}\right), \tan^{-1}\left(\frac{Q_{S2}}{Q_{S1}}\right)\mathrm{sign}\left(a_{x2} - a_{x1}\right) + a_{x1} + Dir, NaN\right), 2\pi\right) \tag{16}$$

where *Qs1*, *Qs2*, *ax1*, and *ax2* are parameters calculated by Equations (12)–(15) and are used to Equation (16). *G* is the orientation angle of the main solar beam. *Dir* is the orientation angle of the car. The function **max2nd**(*A*, *B*, *C*, ...) returns the second largest value from *A*, *B*, *C*, ... The function **mod**(*x*, *y*) returns the remainder on dividing *x* by *y* (*x* modulo *y*). The result has the same sign as *x*. The function **sign**(*x*) returns 0 if $x = 0$, 1 if $x > 0$, and −1 otherwise. Note that Equations (14)–(16) contain Boolean algebra.

Mounting orthogonally-arranged five pyranometers, and applying Equations (8)–(16) to the monitored irradiance data, the three-dimensional solar irradiance around the vehicle may be modeled [17].

2.4. Angular distribution model

The angular distribution of the solar irradiance was calculated by the weighted histogram of the angular distribution. The angular distribution model is crucial both to the validation of the 3-D solar irradiance model around the car-body and optimization design of the high-performance static concentrator module on the car-roof [18-23]. In case that the high-efficiency multi-junction cells are used for VIPV, it is essential to consider the spectrum impact, correctly, the cross effect between spectrum and angular distribution of the solar irradiance [24-32]. The angular distribution model is also useful for this purpose.

The meteorological data and irradiance data are given by the solar irradiance database, specifically, METPV-11 and METPV-Asia [33-35]. It provides both direct and diffused irradiance in every 1 hour. The discrete sampling also makes the distribution shaggy, and for making it continuous, the event time is shifted in the range of plus or minus 30 minutes, also given by the random number under the ranged uniform distribution. The variance of the reflectance by the road and building (or mountains, etc.) also fluctuates the direction of the leading solar beam to the car. The modulation of the reflectance was also given by the random number, precisely, 0.10 to 0.40 for vertical reflection (building or trees), and 0.00 to 0.14 for the horizontal reflection (road).

However, the measurement system defined in Figure 3 does not have enough angular resolution. Instead, the measurement of the incident angle of the main beam was done by the ratio of the vertical irradiance (car-roof) and the highest two irradiances of the car-side, specifically, in equation (10). The validation of the model in the angular distribution in this article is done by comparison of the weighted histogram of the main beam of the solar irradiance using equation (10).

2.5. Curve correction model

The entire formulas and protocols for measurement of the performance of the PV module is based on the preconditions that the PV modules are flat. For example, determination of the output power and other fundamental electrical parameters such as short-circuit current and open-circuit voltage of the PV modules, it is essential to determine the input solar energy to the product of the irradiance and aperture area. On the other hand, the definition of the aperture area for the curved PV is not identical to the surface of the module. The car-roof is three-dimensionally curved, and its curvature may induce power loss by increased cosine loss and self-shading loss [1, 5-10, 14-16, 36]. Another aspect that we need to consider is that the car-roof PV and BIPV (building integrated photovoltaic) are not in the installation of the standard slope angle and orientation. The orientation

Preprints (www.preprints.org) | NOT PEER-REVIEWED | Posted: 2 January 2020 doi:10.20944/preprints202001.0018.v1

of the car-roof changes by time without correlation to the sun direction. Surrounded buildings and other objects often shade both of them. These factors have a different impact on the curve shape. Such interaction is needed to take into account.

We attempt to introduce a simple correction factor that includes complete irradiation loss to the curved surface. We call it the "curve correction factor."

2.5.1 Why is the curved PV modules are often overestimated?

Before discussing the curve-correction, let us clarify where the standard measurement method has a problem. The curved modules are often overestimated. It is because the input energy is often underestimated. The first cause is that the part of the input energy is not detected (Figure 4). Since the illumination area of the solar simulator is always more extensive than the PV module, the curved module will receive unexpected more light coming from the outer region so that it generates unexpected more power.

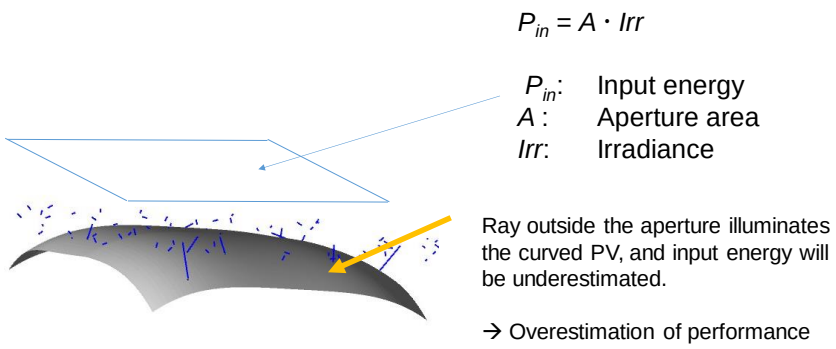

Figure 4. Illustration of the underestimation of the input energy in the measurement of the curved PV module

The second cause is the aperture area of the curved module is not defined clearly (Figure 5). It is a cause of the fatal error in the estimation of the module efficiency in the dividing area of the module.

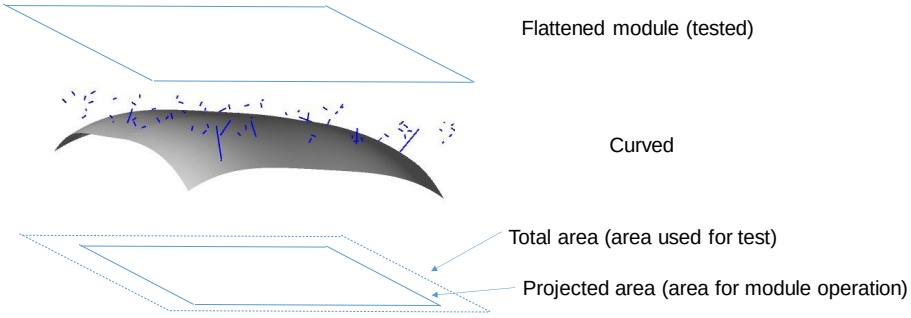

Figure 5. Illustration of the multiple definitions of the module area

The third cause is the difference in the angular distribution in the indoor measurement (typical solar simulator) and outdoor operation. The curved surface generates more loss in the illumination by a higher incident angle (Figure 6).

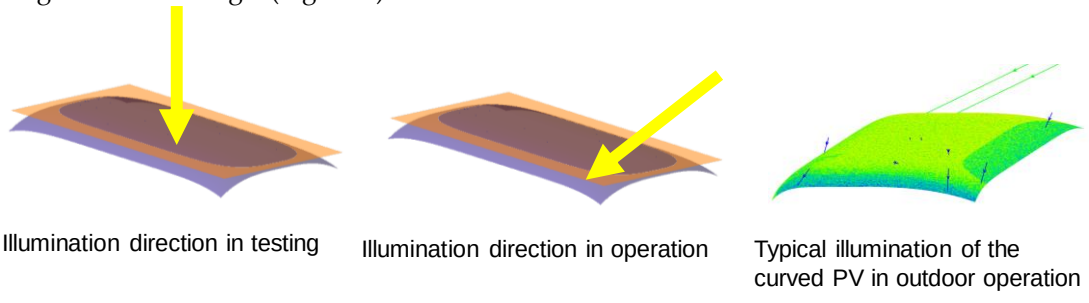

Preprints (www.preprints.org) | NOT PEER-REVIEWED | Posted: 2 January 2020 doi:10.20944/preprints202001.0018.v1

Figure 6. Illustration of the multiple definitions of the module area

2.5.2 Examples of the curve-correction calculations.

A PV module having a curved surface is different from a flat plate module on power output. Specifically, the self-shielding effect of shielding a part of the incident from a shallow angle on its convex surface, the local cosine loss at each point of the solar cell is not constant, and due to the above factors, a mismatching loss further reduces the power output. That is, the output of the curved module has a different output value form the performance test with a conventional solar simulator designed for a flat plate, as we discussed in the previous section. Nonetheless, the exact test method of synthesizing the separately measured outputs by decomposing the curved surface into little surface elements (approximating each surface element to a very flat plate) is scarce in reality [15]. Therefore, a method of considering the power generation output on the 3-D curved surface by multiplying the value measured by assuming the curved module as a 2-D flat plate by the curve correction factor has been studied. This curve correction factor is convenient because it can be uniquely determined for each curved surface given the incidence angle characteristics of the module and the incidence angle distribution of the solar cell if the mismatching loss is neglected.

The curve correction factor can be calculated by numerical, geometric calculation [15] or ray-tracing simulation [1, 6-10, 36]. For the geometrical calculation, it is important to add two conditions for avoiding complexity. First, the module does not absorb the light in the backside. Second, the curved surface is simple convex (no two or more peaks), namely the partial derivative functions of the profile function of the curved surface concerning x and y have no more than 2 points of the zero-crossing.

The curve correction factor f can be defined as equation (17).

$$P = AIf\eta \tag{17}$$

where P is the output of the module, A is a flattened area of the panel (not projected area), I is irradiance of the curved roof, f is the curve-correction factor, and η is the module efficiency measured by the flat condition by the conventional solar simulator. The curve correction factor f is a unique value depending on the 3-D curve shape of the panel if the angular distribution of the solar irradiance is given. It is typically calculated by a numerical calculation (calculation algorithm should be open, transparent, and repeatable within some acceptable numerical errors, i.e., use of the Monte Carlo method). It should apply to the 3-D CAD (computer-aided design) interface (Most of the car-roof 3-D shapes were not simple polynomials but segmented smooth functions).

The curve correction factor f can be expressed as the product of two parameters.

$$f = f_1 f_2 \tag{18}$$

where, f_1 is the coving factor, or in another way, geometrical curve correction factor corresponding to the ratio of the projected area by surface area), f_2 is the irradiance ratio due to the local cosine loss and self-shading loss, in other words, optical curve correction factor. The parameter f_1 may represent the overall shape of the curved surface.

2.5.3 Curve-correction calculation based on ray-tracing simulation.

The basic idea of the curve correction factor is the ratio of the absorbed flux and that of the light source with the area of the projected area of the curved PV panel that is placed just on the curved PV panel (Figure 7). The line segment around the light source (semi-transparent light-blue area) corresponds to the rays emitted from the light source. The short line segments correspond to the ray that does not reach to the curved surface. The longer line segments correspond to the one that hits the curved PV panel (curved opaque gray surface), namely the ray that is absorbed by the PV. Note that some rays just above the curved PV panel do not hit the curved module due to its curvature. To avoid the situation, the real light-source was placed on the surface of the virtual source plane (semi-transparent light-blue area) with the ten times larger area than the virtual light source. A detector is

Preprints (www.preprints.org) | NOT PEER-REVIEWED | Posted: 2 January 2020 doi:10.20944/preprints202001.0018.v1

placed on the virtual light source and measures the total flux that passed the aperture zone (corresponding to the projected area) and compares the total flux absorbed by the curved PV surface (opaque gray surface). Note that the absorption at the backside surface was disabled in this calculation. The angular characteristics of the absorption were assumed as a Lambertian surface.

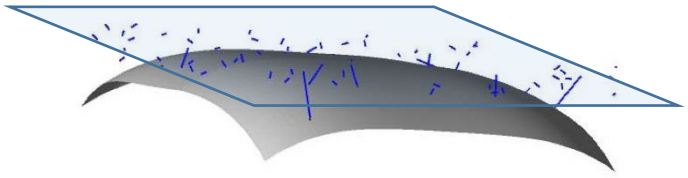

Figure 7. Geometrical relation between the curved PV panel (curved detector, opaque gray surface) and light source (corresponding to the projected area, semi-transparent light-blue area). The line segment around the light source (semi-transparent light-light-blue area) corresponds to the rays emitted from the light source. The short line segments correspond to the ray that does not reach to the curved surface. The longer line segments correspond to the one that hits the curved PV panel (curved opaque gray surface), namely the ray that is absorbed by the PV. Note that rays just above the module do not always hit the module due to its curvature [1].

The curve correction factors of the various shape of the car-roof were calculated and plotted in Figure 8, corresponding each marker in the plot, was given by the random numbers. The curve shape of the car-roof widely varies. Random numbers modeled each surface with an approximation of the bi-cubic spline function structured by the power function of the tangent lines (Fig. 1). The curve shape profile was approximated as the segmented (symmetrical to left-right direction, but asymmetrical to front-back direction) power function constrained by the maximum slope at the edges. Specifically, keeping symmetry in the X direction, but allowing asymmetry in the Y direction, considering that the curve shape of the car-roof may vary in front and tail of the car body. The synthesis calculation is illustrated in Figure 9.

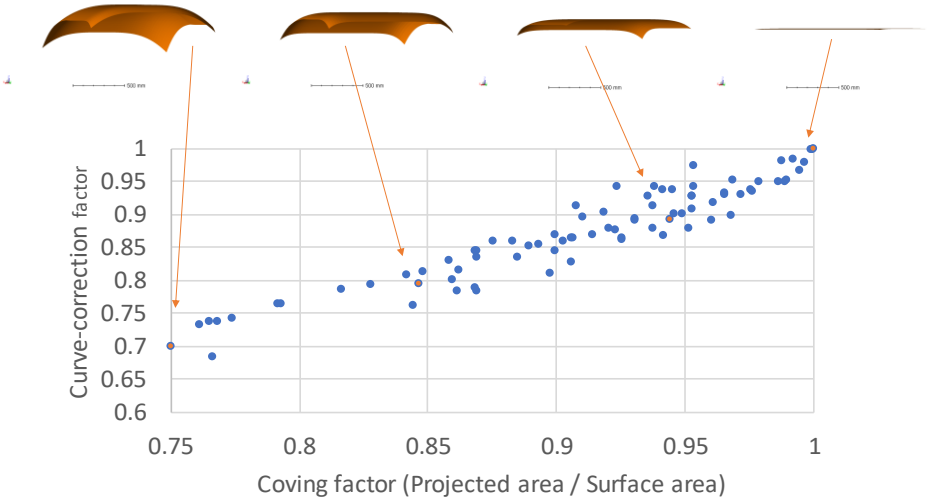

Figure 8. Curve correction factor vs. Representative curve shape parameter (coving factor as f_1)

Preprints (www.preprints.org) | NOT PEER-REVIEWED | Posted: 2 January 2020 doi:10.20944/preprints202001.0018.v1

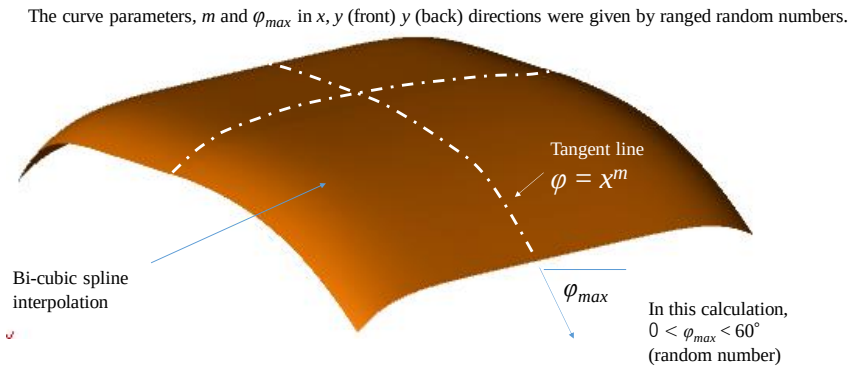

Figure 9. Modeling the curved surface of the car-roof PV using random numbers.

The curve correction factor decreases by the increase of curvature of the surface, corresponding to the ratio of the projected area by surface area (Figure 8). The geometrical factor f_1 dominates it, but the optical curve correction also decreases by the increase of the curvature as well. However, the optical influence depends on the surface shape, and it is essential to calculate its factor to every curve surface.

The above approach can simulate the distribution of the solar irradiance of the curved car-roof PV panel. To do this, it is necessary to specify the orientation of the panel, sun-height, and ratio of the direct and scattered components. It is not appropriate to use the statistical distribution of the incident angle data because the distribution depends on the direction of the direct sunlight.

The distribution of the irradiance varies by both sun-height and orientation angle. Unlike the BIPV, the orientation angle of the car-roof PV varies by time. Such non-uniformity was observed by the measurement of the mini-module attached to various places on the car-roof [11-13, 23].

To avoid complexity, the validation by the measurement in this article did not consider the non-uniformity and the resultant mismatching loss in the module, but only considered the total flux absorbed by the module. The mismatching loss is handled separately by a Monte Carlo simulation, but it is not validated in this article. Although the mismatching loss due to non-uniformity may be expected, it will be significantly relaxed by the appropriate string design [14], and thus less significant than the reduction of the total flux.

The curve correction factor is also affected by the angular distribution of the solar irradiation. Roughly, the angular distribution of the sunlight in the horizontal surface moves to the higher incident angle, when the sun-height is low, thus higher latitude, the lower average height of the shading objects, and the seasonal fluctuation of the sunshine duration high in winter.

The curve correction factors, f, and f_2, significantly vary by the site conditions, including latitude, climate pattern, and shading environment (urban zone or rural zone). This is because of the difference in the distribution of the incident angle onto the curved surface (Figure 10).

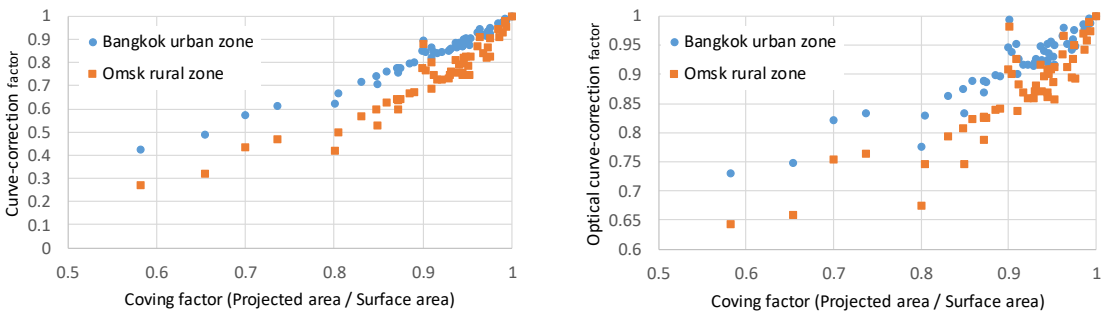

Figure 10. Curve correction factor vs. Representative curve shape parameter (coving factor as f1) in two extreme cases. One is the urban zone in Bangkok (N13.7°and 4.87 kWh/m2/day GHI), drawn by

Preprints (www.preprints.org) | NOT PEER-REVIEWED | Posted: 2 January 2020 doi:10.20944/preprints202001.0018.v1

a blue line, and another is a rural zone of Omsk (N54.9°and 3.34 kWh/m2/day GHI) drawn in orange line. : (**a**) curve-correction factor f; (**b**) optical curve correction factor f_2.

2.6. Partial and dynamic shading modell

The shading influence is complicated and varies by the position and the relative orientation (to the sun position) of the panel. In the case of the car-roof PV, the position (orientation) of the panel cannot be predicted. One practical approach is to rely on the probability model, supposing that the distribution and height of the shading objects are randomly distributed by some statistical model and the orientation of the car is independent and random as well.

Most of the PV on the car-roof is curved, thus induces the non-uniform illumination caused by areal variation of the local cosine loss and self-shading loss. Such non-uniform illumination caused by the curved surface is equivalent to the partial shading given non-uniform photo-current output from each solar cell. A ray-tracing simulation can estimate such non-uniformity.

The above approach can simulate the distribution of the solar irradiance of the curved car-roof PV panel. To do this, it is necessary to specify the orientation of the panel, sun-height, and ratio of the direct and scattered components. It is not appropriate to use the statistical distribution of the incident angle data because the distribution depends on the direction of the direct sunlight.

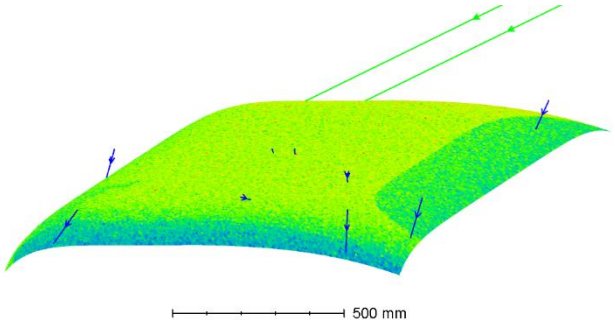

Figure 11. Solar irradiance distribution on the curved surface of the PV panel. The light-green arrow lines correspond to the direct sunlight. The blue arrow lines correspond to the scattered sunlight. The color gladiation on the curved surface indicates the non-uniformity of the irradiance on the curved surface. The darker color indicates the lower irradiance.

The distribution of the irradiance varies by both sun-height and orientation angle. The orientation angle of the car-roof PV varies by time. Such non-uniformity was observed by the measurement of the mini-module attached to various places on the car-roof [13-15].

As was discussed in the previous sections, car-roof PV often partially shaded or receives equivalent non-uniform illumination caused by its basic curved shape. Both partial shading and non-uniform illumination can be simultaneously and quantitatively modeled, considering that both primary effect to the variation of short-circuit current of the cells.

For simplicity, cells in a module were categorized into three types.

1. In the sun
2. Full shade
3. Partial shade

Cells in the sun were supposed to be illuminated by all the sunlight, including the direct sunlight, but the shaded cells would not receive the direct component of the sunlight but would receive (Diffused sunlight) + (Reflected sunlight).

Random numbers gave the number of the shaded cells (both full shaded and partially shaded) with some constraints. Random numbers also gave the ratio of the shaded area of each partially-shaded cells. Random numbers gave the position of the sun that affects the angle of the sunbeam and the orientation of the car-roof as well. Finally, the I-V curve of each cell was calculated by three randomly distributed three parameters (normal distribution). The property of the probability

Preprints (www.preprints.org) | NOT PEER-REVIEWED | Posted: 2 January 2020 doi:10.20944/preprints202001.0018.v1

variables used for the Monte Carlo simulation is summarized in Table 1. The irradiance and climate conditions corresponding to the above parameters were looked into in the database of METPV-11 and METPV-Asia [33-35]. Given those probability parameters, I-V curves of entire cells in the array affected different illumination conditions, and variations of characteristics were calculated, and the maximum power point was calculated for taking the simulated power output affected by the partial shading.

Table 1. Summary of random variables used to the Monte Carlo simulation.

Section	**Distribution**	**Type**	**Range**
Date (Day number)1	Uniform distribution	Integer	0 – 364 (day)
Time[1]	Uniform distribution	Integer	0 – 23 (hour)
Number of cells partially shaded[2]	Uniform distribution	Integer	0 – (Number of cells in the string)
Number of cells fully shaded2	Uniform distribution	Integer	0 – (Number of cells in the string)
Shading ratio of each partially-shaded cell3	Uniform distribution	Real	0 - 1
Car orientation4	Uniform distribution	Real	0°- 360°
Isc of each cell	Normal distribution	Real	--
Voc of each cell	Normal distribution	Real	--
Diode ideality5	Normal distribution	Real	Greater than 1

[1] Repeat throwing a dice until the horizontal global sunlight given by the database is more than 1 Wh/m^2 to avoid the inclusion of the trial in the night time. The bissextile day is removed.

[2] Random numbers are given to each string. The number of partial and full shaded cells must be less than the number in the strings.

[3] The ratio of the partial shading (0 to 1)

[4] Assuming that the car always parks or runs on the horizontal plane.

[5] Representing the shape of the I-V curve

It is important to note that the probability modeling of the partial shading, corresponding to the forth to sixth rows of Table 2, is the key to the simulation. For minimizing the evil influence of the partial shading, the PV and car manufacturers try to place the series strings as close to the shape of the partial shading or non-uniform illumination pattern caused by the curvature of the car-body as possible, In a way, the distribution of the shaded cells are not uniformly distributed but leaves some distribution pattern. To mimic this situation, the random model was made by three steps (see 4th to sixth rows of Table 1). Specifically, the number of the shaded cells in each string was allocated using Equation (19), and the short-circuit current from each cell impacted by shading was given in equation (2). Note both equation (1) and equation (2) contains Boolean algebra. It is also important to note that the vector and matrix data that were generated by the above calculation and contains the information of the shaded ratio of each cell in the module is only used as the circuit calculation of the module by series-parallel connection with bypass diodes. Therefore, in the downstream calculation step, the position of the shaded cell is not referred, but they may be redistributed in the series connection by order of the shaded ratio.

Preprints (www.preprints.org) | NOT PEER-REVIEWED | Posted: 2 January 2020 doi:10.20944/preprints202001.0018.v1

$$SF(n, Nstrings) := \left\| \begin{array}{l} \text{if } Nstrings < 2 \\ \quad u_0 \leftarrow \text{floor}(\text{rnd}(n)) \\ \text{else} \\ \quad v_0 \leftarrow \text{floor}(\text{rnd}(n)) \\ \quad \text{for } i \in 1 .. Nstrings - 1 \\ \quad\quad sum \leftarrow \sum_{j=1}^{i} v_{j-1} \\ \quad\quad v_i \leftarrow \text{if}(n - sum > 0, \text{floor}(\text{rnd}(n - sum)), 0) \\ \quad\quad v \leftarrow \text{stack}(v, v_i) \\ \quad u \leftarrow \text{submatrix}(v, 0, Nstrings - 1, 0, 0) \\ \quad u_0 \leftarrow n - \sum_{j=1}^{Nstrings-1} u_j \\ \quad u \end{array} \right\| \tag{19}$$

$$Ir_{i,j} := \frac{STI + \left(\left(j < Scn_i \right) + \text{if}\left(\left(Scn_i \le j < Snp_i + Scn_i \right) \wedge Snp_i > 0, \text{runif}\left(Snp_i, 0, 1 \right)_{j - Scn_i}, 0 \right) \right) \cdot DTI}{TIS} \tag{20}$$

where, **SF**(*n*, *Nstrings*) is a function that generates a vector containing the number of shaded cells in each string. n is a scalar parameter of the number of the cells in a string. *Nstrings* is a scalar parameter of the number of the strings in a module. **floor**(*z*) is a function that returns the greatest integer ≤ *z*. **rnd**(*x*) is a function that returns a uniformly distributed random number between 0 and *x*. **if**(*cond*, *x*, *y*) is a function returns *x* if *cond* is true (nonzero), *y* otherwise. **stack**(*A* , *B*, *C*, ...) is a function that returns an array formed by placing *A*, *B*, *C*, ... top to bottom. **submatrix**(**A**, *ir*, *jr*, *ic*, *jc*) is a function that returns the matrix consisting of rows *ir* through *jr* and columns *ic* through *jc* of array **A**. **Ir** in Equation (20) is an array that contains solar irradiance of each cell in the module affected by partial shadings. *STI* is a scalar parameter of the diffused sunlight onto the module plane. **Scn** is a vector that contains a number of the unshaded cells in each string in the module. **Snp** is a vector that contains a number of partially shaded cells in strings. **runif**(*m*, *a*, *b*) is a function that returns a vector of *m* random numbers having the uniform distribution, and *m* is a scalar of real values, $a \le m \le b$. To allow integration and other operations over this argument, values outside of the stated range are allowed, but they produce a 0 result. *a* and *b* are real numbers, $a < b$. *DTI* is a scalar parameter of the direct sunlight onto the module plane. *TIS* is a scalar parameter of the total sunlight onto the module plane.

3. Results

In this article, we evaluated the annual irradiance incident on the car using five pyranometers located in five orthogonal directions. We also presented the seasonal variation of the angular distribution of the leading solar beam and the annually angular distribution model on car-roof.

3.1. 3-D measurement by multiple pyranometer array

The measurement system consisted of five pyranometers mounted on the car roof, along with a GPS, and thus, could be moved on the road. The pyranometer axes Q_{x+}, Q_{x-}, Q_{y+}, Q_{y-}, and Q_z were defined as shown in Figure 1and 12. One pyranometer was placed horizontally on the car roof (Q_z), and four pyranometers were placed vertically facing each side of the car (Q_{x+}, Q_{x-}, Q_{y+}, Q_{y-}). The global irradiance onto the car roof (I_z) was measured using a pyranometer Q_z. The global irradiance onto the side of the car (I_{x+}, I_{x-}, I_{y+}, I_{y-}) was measured using pyranometers Q_{x+}, Q_{x-}, Q_{y+}, Q_{y-}. The direction of the moving car was equal to that of Q_{y+}. An ambient temperature meter (Pt 100 temperature sensor) was also placed on the car roof. The GPS was incorporated into the data logger, and data was recorded in 1 s intervals. The total number of hours of sun radiation (more than 10 W/m² in I_z) received over the year was 3374 h, while the number of hours the car was running was approximately 6% of this.

To acquire a dataset for comparison, a conventional static irradiance measurement system with a pyrheliometer, a tracking pyranometer mounted onto a sun tracker, a horizontal pyranometer, and

Preprints (www.preprints.org) | NOT PEER-REVIEWED | Posted: 2 January 2020 doi:10.20944/preprints202001.0018.v1

two vertical pyranometers facing eastward and westward was installed at the University of Miyazaki, Japan (31°49′N, 131°24′E). The elevation angle and azimuth angle of the sun position were calculated based on the conventional method, including the day angle, declination angle, time equation, hour angle, latitude, and longitude.

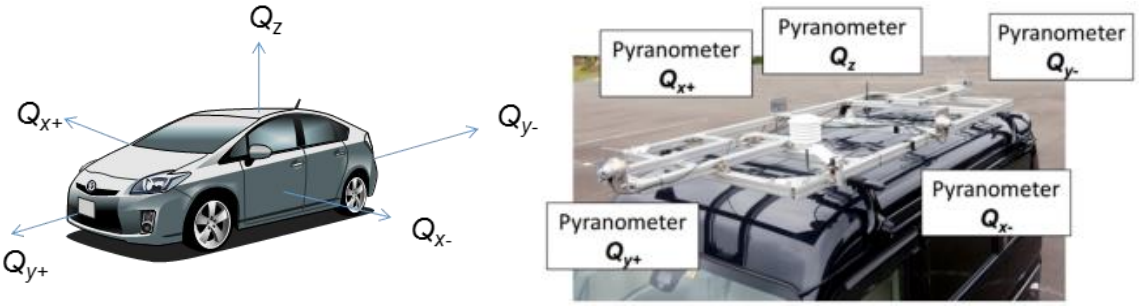

Figure 12. Measurement system on the car using five pyranometers on the orthogonal axis.

3.2 Measurement example of the solar irradiance on the car-roof and car-side

The city of Miyazaki, Japan, is one of the capitals of local government in Japan (Miyazaki prefecture) with approximately 200 thousand population. Thus, this area contains an urban zone, a residential zone and a rural zone. In a way, it may be a representative zone in the solar environment (shading frequency and shading height). We did not constrain the driving course of the one-year monitoring of the solar irradiance on the car, but the most frequent driving course of this car is shown in Figure 13 since it was used for commuting between the University of Miyazaki and driver's residence.

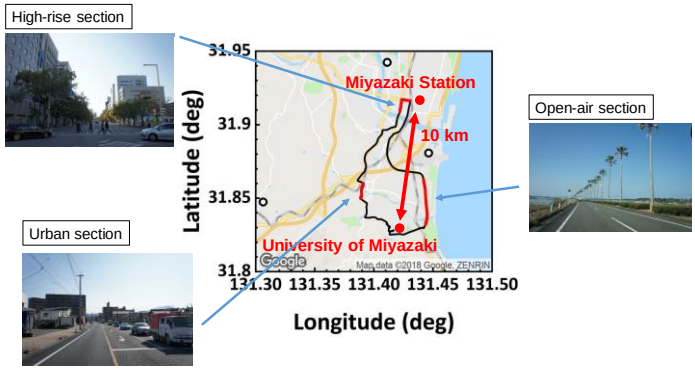

Figure 13. Most-frequent driving course of the dynamic solar irradiance measurement in the car.

The typical monitored result in the route in Figure 13 is shown in Figure 14 (clear sky day) with comparison to the GHI of fixed pyranometers (mounted on a roof of one of the buildings of the University of Miyazaki).

In the region of the open-air section, the solar irradiance on the car-roof was almost identical to the GHI by the fixed pyranometers. However, that of other areas had frequent dips in the irradiance on the car. The timestamp and position data taken by GPS confirmed that these were because of the shading effects by buildings and mountains. The car-roof irradiance often exceeded GHI. It was also confirmed because of the reflectance of the buildings.

Preprints (www.preprints.org) | NOT PEER-REVIEWED | Posted: 2 January 2020 doi:10.20944/preprints202001.0018.v1

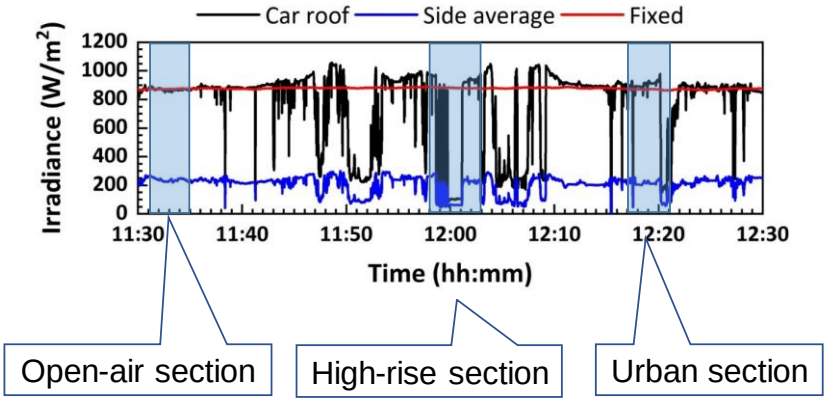

Figure 14. Monitored the result of the solar irradiance on the car-roof and car-sides in the driving route in Figure 13.

3.3 Validation of the solar irradiation model around the car (intensity)

The above model was compared with the one-year observation result of the solar irradiance to the vehicle, including seasonal (monthly) fluctuation. After fitting to the measurement irradiance dataset, the fitted average shading height was 18.7° in the direction along the road (local axis) and 12.3°in the direction orthogonal to the road (local axis), and 15.5° as the average. The averaged shading height after data fit was 15.5° and it was very closed from the value of rough physical measurement (15° on average). The average reflectance from the road was also fit to the measured data and was obtained as 0.088, also reasonable value for aged asphalt (typical value is 0.07). The comparison to the measured irradiance and modeled irradiance were compared in Table 2.

Table 2. Comparison of model and measurement (relative to GHI) by one-year monitoring of a passenger's car

	Measured	Model by rough physical measurement	Modeled by parameter fit (average height of shading objects and reflectance of the road)[1]
Car-roof	0.925	0.929	0.925
Car-side (x-direction)	0.395	0.412	0.395
Car-side (y-direction)	0.435		0.435

[1] The degree of freedom and the number of fit parameters are the same (= 3).

The validation was also done by a one-month integration (seasonal fluctuation). The model met the modeled values in every month (Figure 14). The trend of the residual errors could be explained by the difference in climate from the regular year (for example, cloudy in summer).

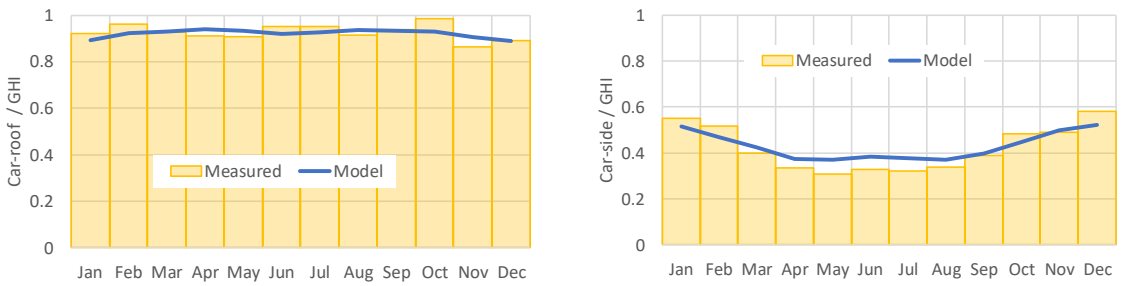

(a) (b)

Figure 14. Monthly-based comparison between the measured solar irradiance around the car (bar-chart) and modeled (typical year from the METPV-11 solar database) solar irradiance on the car (line-chart): (**a**) car-roof irradiance; (**b**) car-side irradiance.

Preprints (www.preprints.org) | NOT PEER-REVIEWED | Posted: 2 January 2020 doi:10.20944/preprints202001.0018.v1

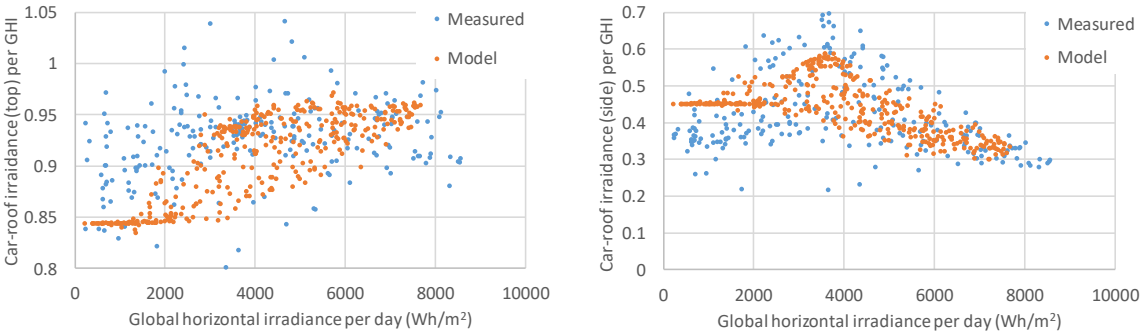

(a) (b)

Figure 15. Daily-based comparison between the measured solar irradiance around the car (blue dots) and modeled (typical year from the METPV-11 solar database) solar irradiance on the car (orange dots): (**a**) car-roof irradiance; (**b**) car-side irradiance.

The same comparison was made in daily-base (Figure 15). Since every day's climate was not always identical to the one in the solar database, there were significant errors in the time-series trend. However, the range of the distribution in the modeled irradiance was almost the same as the measured irradiance.

3.4 Validation of the solar irradiation model around the car (Angle)

After validation of the irradiance model affected by the surrounding shading objects, the histogram of the car irradiance was counted using the one-year irradiation model. The results of annually integrated angular distribution were shown in Figure 16. For examining the seasonal trend, the weighted histograms of the angular distribution of the leading solar beam in each month were plotted in Figure 17. The residual error of the model was observed in more than 30° of incident angle or winter season (corresponding low sun-height and high incident angle). It is possible because the model of the shading height distribution was too simplified. However, the overall trend met the measured one, and the angular model can be used for a rough estimation of the solar irradiance environment around the car-body.

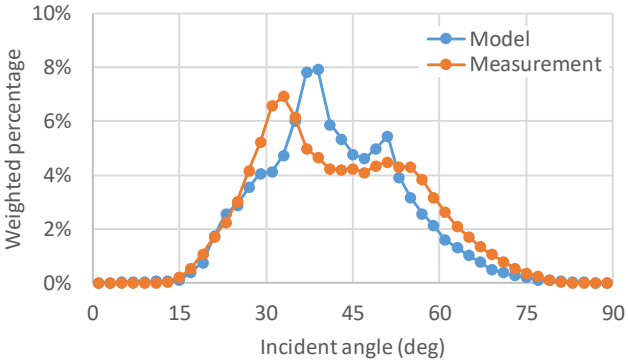

Figure 16. Annually-integrated angular distribution (weighted histogram of the leading solar beam).

Preprints (www.preprints.org) | NOT PEER-REVIEWED | Posted: 2 January 2020 doi:10.20944/preprints202001.0018.v1

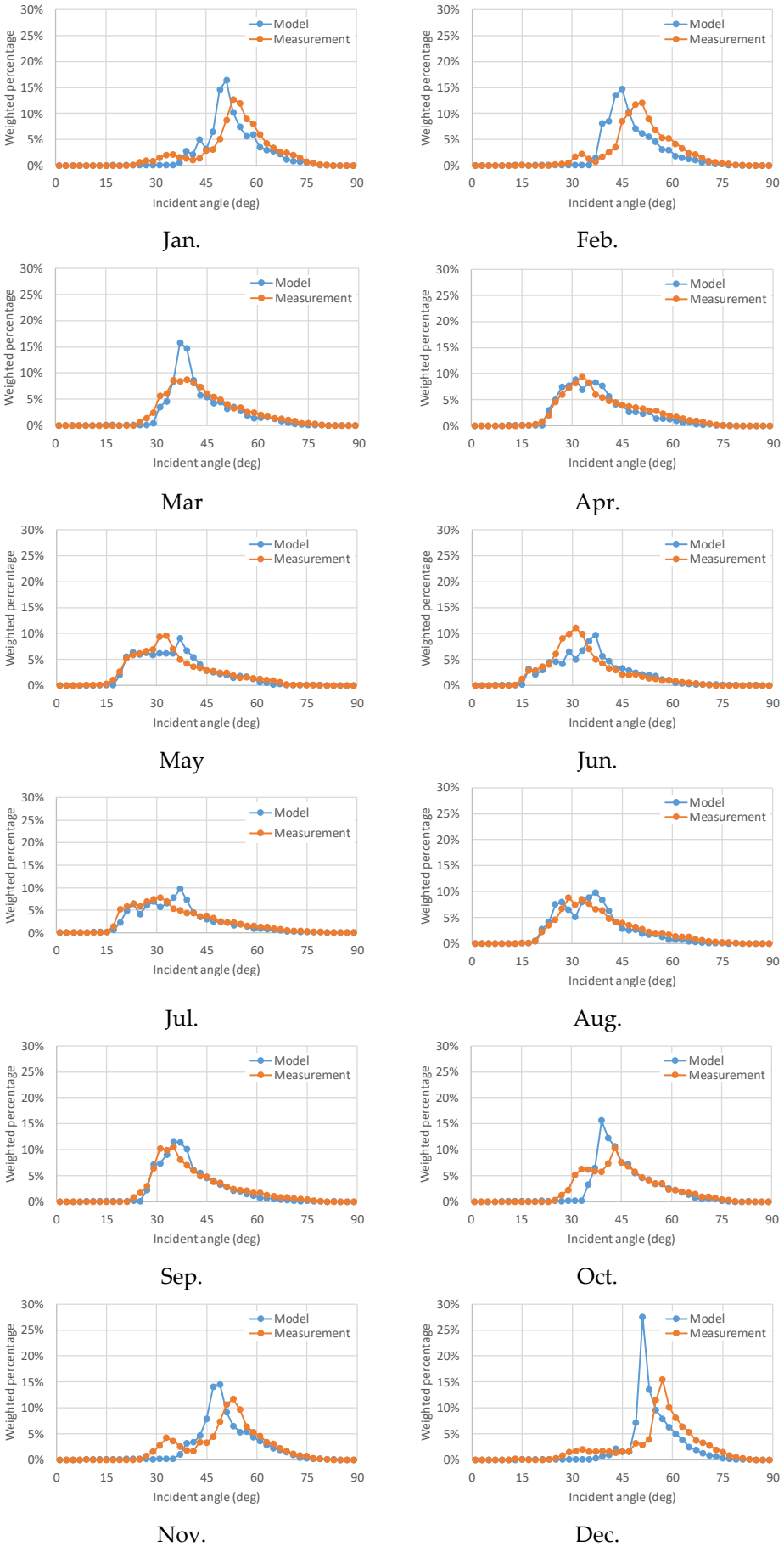

Figure 16. Monthly-integrated angular distribution (weighted histogram of the leading solar beam).

Preprints (www.preprints.org) | NOT PEER-REVIEWED | Posted: 2 January 2020 doi:10.20944/preprints202001.0018.v1

4. Discussion.

4.1. Simplified rating method of VIPV considering 3-dimensional solar irradiance

The standard rating measurement for PV is done by a single measurement in the normal illumination. However, that of VIPV is not sufficient because it uses three-dimensional solar irradiance by curved module and three-dimensional installation (frequently, the PV module on the car-side is added).

The ratio of solar resource measurement is useful for a quick rating of the VIPV system on the car by three-dimensional measurement. A possible step is as follows:

1. Measure the PV performance in 5 directions (see Figure 2).
2. The rating of the total performance in the specific area can be weighted by the normalized solar resources using Equation (21) and the values in Table 2, namely,

$$P = aP_z + b(P_{x+} + P_{x-}) + c(P_{y+} + P_{y-}) \quad (21)$$

where, P is the rated power output. P_z is the measured power output by the illumination on the car-roof. P_{x+}, P_{x-}, P_{y+}, and P_{y1} are the measured power outputs by the illumination on the car-sides in the direction defined in Figure 1. a, b, and c are weighting coefficient given by Table 2. Note that the coefficients a, b, and c in our measurement in Miyazaki, Japan is 0.925, 0.395, and 0.435. The Equation (21) gives a total energy output of the entire PV system on the vehicle considering 3-D solar irradiance around the vehicle comparable to GHI.

4.2. Estimation of the practical solar resource to VIPV in other regions

Assuming that the density and height distribution of the shading objects are the same to that of Miyazaki, Japan, namely the average shading height is about 15.5°, it may be possible to anticipate the energy yield of the VIPV in various area in the world, that is useful to anticipate the merits of the introduction of the solar-driven vehicles.

Figure x indicates the map of the practical solar resource on the car-roof normalized to the GHI, affected by climate conditions. They were calculated using a model in section 2.2 and 2.5, using METPV-ASIA solar irradiance database. Due to the shading impact and curved surface, the practical solar resource for the car-roof is less than the typical installation. The rough value maybe 3/4 of the GHI.

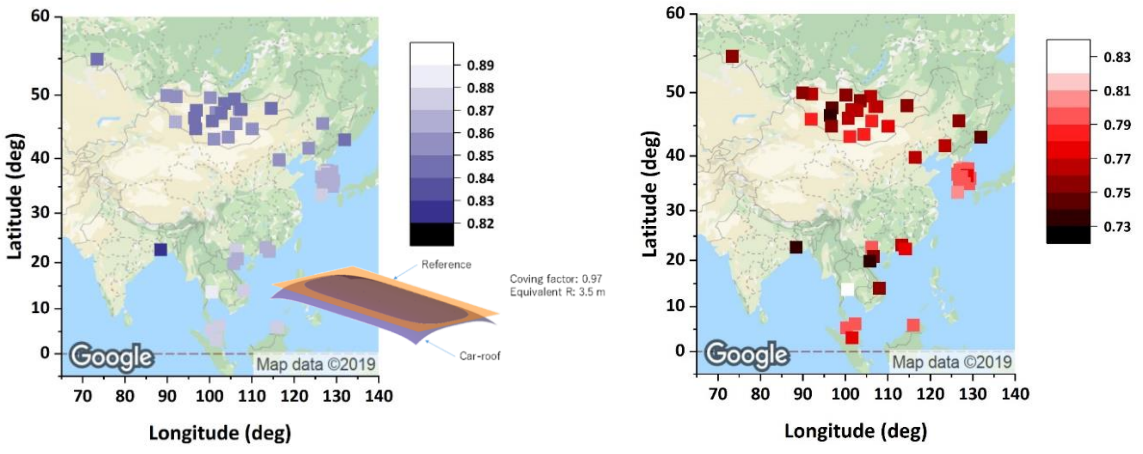

(**a**) (**b**)

Figure 17. Map of the effective solar irradiance for the car-roof: (**a**) Curve-correction factor in typical car-roof; (**b**) Effective solar resource to the car-roof normalized to GHI, including the loss by the curved surface.

4.3. Simplified rating method of VIPV considering 3-dimensional solar irradiance

Preprints (www.preprints.org) | NOT PEER-REVIEWED | Posted: 2 January 2020 doi:10.20944/preprints202001.0018.v1

Since calculated power and related loss were affected by probability variables, the calculated result was not a single number but showed distribution. Fig. 8 shows an example of the distribution of the normalized efficiency of several array designs of the car-roof PV, affected by the mismatching loss result from partial shading. The ratio of the power output of the partially shaded module is less than the ratio of the area in the sun. The reduction ratio corresponds to the mismatching loss. The loss factor is a function of the number of strings, curvature of the car-roof and latitude.

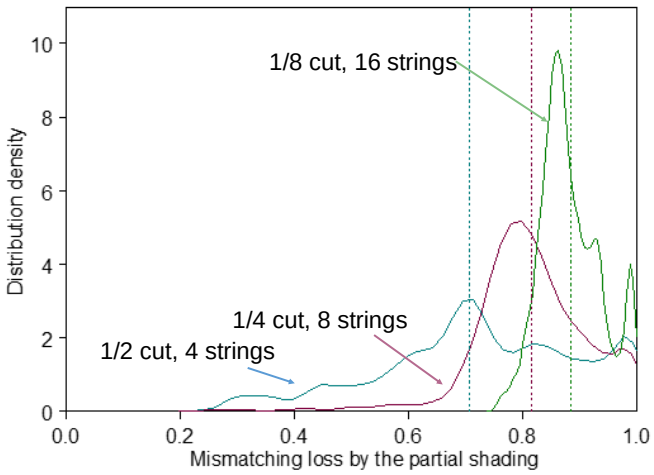

Figure 18. Distribution of the normalized efficiency of some design of the car-roof PV affected by synthesized partial shading given by the Monte Carlo simulation. Note 1/6 or more cut is recommended for suppressing partial-shading loss to < 10%.

4.4. Future works

For improvement of the energy yield prediction of VIPV, the following works are to be done.

1. Improvement of the shading model. The current model is useful but too simplified, especially in the urban area. Note that more than 45° of the average shading height is not allowed, because the maximum height becomes more than 90°. Even in the area of Miyazaki, the average height of 15.5° means that the maximum height should be 31°. However, there were many buildings of more than 31°. Possibly, we need to develop a curved trend, namely the two parameters model.
2. Modeling of partial shading validated to the measured data. To do this, we need to start monitoring the partial shading on the car-roof and car-body.
3. Validation of energy yield using the real curved PV module.
4. Validation of the shading model by several areas with different shading height and shading density.
5. Development of the spectrum model for predicting energy yield by multi-junction solar cells on the car-roof and car-body.

5. Conclusions

1. A simple shading model to VIPV was developed and validated by one-year monitoring on the solar irradiation on the car-roof and car-body in 5 axes.
2. The curve-correction model of the curved surface of VIPV was developed.
3. Mismatching model using Monte Carlo simulation was developed to analysis on the partial shading of VIPV.

Author Contributions: Conceptualization, K.A.; methodology, Y. O.; software, K.A.; validation, Y.O.; investigation, Y.O.; data curation, Y.O.; writing—original draft preparation, K.A.; writing—review and editing, Y.O.; visualization, K.A., and Y.O.; supervision, Y.O.; project administration, M.Y.; funding acquisition, M.Y.

Preprints (www.preprints.org) | NOT PEER-REVIEWED | Posted: 2 January 2020 doi:10.20944/preprints202001.0018.v1

Funding: Part of this research was funded by the New Energy and Industrial Technology Development Organization (NEDO) under the Ministry of Economy, Trade, and Industry (METI), Japan.

Acknowledgments: The modeling of VIPV was first discussed in the international web meetings (76 scientists and engineers are registered) for the standardization of the car-roof PV, starting discussions in December 2017. Part of this research was funded by NEDO, Japan. The standardization activities was supported by JEMA, Japan.

Conflicts of Interest: The authors declare that there is no conflict of interest.

References

1. Araki, K.; Ji, L.; Kelly, G.; Yamaguchi, M. To Do List for Research and Development and International Standardization to Achieve the Goal of Running a Majority of Electric Vehicles on Solar Energy. *Coatings* **2018**, *8*, 251.
2. Masuda, T.; Araki, K.; Okumura; K.; Urabe, S.; Kudo, Y.; Kimura, K.; Nakado, T.; Sato, A.; Yamaguchi, M.; Static concentrator photovoltaics for automotive applications. Solar Energy **2017**, 146, 523-531.
3. NEDO, Interim Report of the Exploratory Committee on the Automobile Using Photovoltaic System.
4. Masuda, T.; Araki, K.; Okumura, K.; Urabe, S.; Kudo, Y.; Kimura, K.; Nakado, T.; Sato, A.; Yamaguchi, M. Next environment-friendly cars: Application of solar power as automobile energy source. In Proceedings of the 2016 IEEE 43rd Photovoltaic Specialists Conference (PVSC), Portland, OR, USA, 5–10 June 2016; pp. 0580–0584.
5. Araki, K.; Sato, D.; Masuda, T.; Lee, KH.; Yamada, N.; Yamaguchi, M. Why and how does car-roof PV create 50 GW/year of new installations? Also, why is a static CPV suitable to this application?. InAIP Conference Proceedings **2019** Aug 26 (Vol. 2149, No. 1, p. 050003). AIP Publishing.
6. Araki, K.; Ota, Y.; Nishioka, K.; Tobita, H.; Ji, L.; Kelly, G.; Yamaguchi , M., Toward the Standardization of the Car-roof PV – The challenge to the 3-D Sunshine Modeling and Rating of the 3-D Continuously Curved PV Panel. IEEE 7th World Conference on Photovoltaic Energy Conversion (WCPEC) (A Joint Conference of 45th IEEE PVSC, 28th PVSEC & 34th EU PVSEC) **2018**, 0368-0373. 10.1109/PVSC.2018.8547925.
7. Araki, K.; Algora, C.; Siefer, G.; Nishioka, K.; Leutz, R.; Carter, S.; Wang, S.; Askins, S.; Ji, L.; Kelly, G. Standardization of the CPV and car-roof PV technology in 2018–Where are we going to go? *Aip Conf. Proc.* **2018**, *2012*, 070001.
8. Araki, K.; Algora, C.; Siefer, G.; NIshioka, K.; Muller, M.; Leutz, R.; Carter, S.; Wang, S.; Askins, S.; Ji, L.; et al; Toward Standardization of Solar trackers, concentrator PV, and car-ROOF pv. *Grand Renew. Energy Proc. Jpn. Counc. Renew. Energy* **2018**, *2018*, 37.
9. Araki K, Algora C, Siefer G, Nishioka K, Leutz R, Carter S, Wang S, Askins S, Ji L, Kelly G. Standardization of the CPV technology in 2019–The path to new CPV technologies. InAIP Conference Proceedings 2019 Aug 26 (Vol. 2149, No. 1, p. 090001). AIP Publishing.
10. Ota, Y.; Masuda, T.; Araki, K.; Yamaguchi, M., Curve-Correction Factor for Characterization of the Output of a Three-Dimensional Curved Photovoltaic Module on a Car Roof. Coatings **2018**, 8(12), 432.
11. C. Schuss, T. Kotikumpu, B. Eichberger, T. Rahkonen, "Impact of dynamic environmental conditions on the output behaviour of photovoltaics", Proceedings of the 20th IMEKO TC-4 International Symposium, pp. 993–998, 2014.
12. Schuss, C.; Gall, H.; Eberhart, K.; Illko, H.; Eichberger, B. Alignment and interconnection of photovoltaics on electric and hybrid electric vehicles. In Proceedings of the 2014 IEEE International Instrumentation and Measurement Technology Conference (I2MTC) Proceedings, Montevideo, Uruguay, 12–15 May 2014; pp. 153–158.
13. Schuss, C.; Eichberger, B.; Rahkonen, T. Impact of sampling interval on the accuracy of estimating the amount of solar energy. In Proceedings of the IEEE International Instrumentation and Measurement Technology Conference Proceedings, Taipei, Taiwan 23–26 May 2016; pp 1–6.
14. Araki, K.; Lee, K-H.; Masuda, T.; Hayakawa, Y.; Yamada, N.; Ota, Y.; Yamaguchi, M. Rough and Straightforward Estimation of the Mismatching Loss by Partial Shading of the PV Modules Installed on an Urban Area or Car-Roof, 2019, In 46th IEEE PVSC, in press.
15. Tayagaki, T.; Araki, K.; Yamaguchi, M.; Sugaya, T., Impact of Nonplanar Panels on Photovoltaic Power Generation in the Case of Vehicles. 2019, IEEE Journal of Photovoltaics, 9(6), 1721-1726.

Preprints (www.preprints.org) | NOT PEER-REVIEWED | Posted: 2 January 2020 doi:10.20944/preprints202001.0018.v1

16. Araki, K.; Ota, Y.; Lee, K-H.; Y.; Yamada, N.; Yamaguchi, M. Curve Correction of the Energy Yield by Flexible Photovoltaics for VIPV and BIPV Applications Using a Simple Correction Factor, 2019, In 46th IEEE PVSC, in press.
17. Ota, Y.; Masuda, T.; Araki, K.; Yamaguchi, M. A mobile multipyranometer array for the assessment of solar irradiance incident on a photovoltaic-powered vehicle. *Sol. Energy*. **2019**, *184*, 84–90.
18. Araki, K.; Ota, Y.; Ikeda, K.; Lee, K.H.; Nishioka, K.; Yamaguchi, M. Possibility of static low concentrator PV optimized for vehicle installation. *Aip Conf. Proc.* **2016**, *1766*, 020001.
19. Ota, Y.; Nishioka, K.; Araki, K.; Ikeda, K.; Lee, K.H.; Yamaguchi, M. Optimization of static concentrator photovoltaics with aspherical lens for automobile. In Proceedings of the IEEE 43rd Photovoltaic Specialists Conference (PVSC), Portland, OR, USA, 5–10 June 2016; pp. 0570–0573.
20. Araki, K.; Lee, K.H.; Yamaguchi, M. The possibility of the static LCPV to mechanical-stack III-V//Si module. *Aip Conf. Proc.* **2018**, *2012*, 090002.
21. Sato, D.; Lee, K.H.; Araki, K.; Masuda, T.; Yamaguchi, M.; Yamada, N. Design and Evaluation of Low-concentration Static III-V/Si Partial CPV Module for Car-rooftop Application. In Proceedings of the IEEE 7th World Conference on Photovoltaic Energy Conversion (WCPEC) (A Joint Conference of 45th IEEE PVSC, 28th PVSEC & 34th EU PVSEC), Waikoloa Village, HI, USA, 10–15 June 2018; pp. 0954–0957.
22. Araki K, Lee KH, Yamaguchi M. The possibility of the static LCPV to mechanical-stack III-V//Si module. InAIP Conference Proceedings 2018 Sep 13 (Vol. 2012, No. 1, p. 090002). AIP Publishing.
23. Sato, D.; Lee, K.H.; Araki, K.; Masuda, T.; Yamaguchi, M.; Yamada, N. Design of low-concentration static III-V/Si partial CPV module with 27.3% annual efficiency for car-roof application. *Prog. Photovolt. Res. Appl.* **2019**, 27, *6*, 501–510.
24. Araki, K.; Ota, Y.; Lee, K.H.; Nishioka, K.; Yamaguchi, M. Optimization of the Partially Radiative-coupling Multi-junction Solar Cells Considering Fluctuation of Atmospheric Conditions. In Proceedings of the IEEE 7th World Conference on Photovoltaic Energy Conversion (WCPEC) (A Joint Conference of 45th IEEE PVSC, 28th PVSEC & 34th EU PVSEC), Waikoloa Village, HI, USA, 10–15 June 2018; pp. 1661–1666.
25. Araki, K.; Ota, Y.; Saiki, H.; Tawa, H.; Nishioka, K.; Yamaguchi, M. Super-Multi-Junction Solar Cells—Device Configuration with the Potential for More Than 50% Annual Energy Conversion Efficiency (Non-Concentration). Appl. Sci. 2019, 9, 4598.
26. Saiki, H.; Sakai, T.; Araki, K.; Ota, Y.; Lee, K.H.; Yamaguchi, M.; Nishioka, K. Verification of uncertainty in CPV's outdoor performance. In Proceedings of the IEEE 7th World Conference on Photovoltaic Energy Conversion (WCPEC)(A Joint Conference of 45th IEEE PVSC, 28th PVSEC & 34th EU PVSEC), Waikoloa Village, HI, USA, 10–15 June 2018; pp. 0949–0953.
27. Araki, K.; Ota, Y.; Lee, K.H.; Sakai, T.; Nishioka, K.; Yamaguchi, M. Analysis of fluctuation of atmospheric parameters and its impact on performance of CPV. Aip Conf. Proc. 2018, 2012, 080002.
28. Araki, K.; Lee, K.H.; Yamaguchi, M. Impact of the atmospheric conditions to the bandgap engineering of multi-junction cells for optimization of the annual energy yield of CPV. Aip Conf. Proc. 2017, 1881, 070002.
29. Araki, K.; Ota, Y.; Lee, K.H.; Nishioka, K.; Yamaguchi, M. Improvement of the Spectral Sensitivity of CPV by Enhancing Luminescence Coupling and Fine-tuning to the Bottom-bandgap Matched to Local Atmospheric Conditions. Aip Conf. Proc. 2019, 2149, 060001.
30. Araki, K.; Ota, Y.; Sakai, T.; Lee, K.H.; Nishioka, K.; Yamaguchi, M. Energy yield prediction of multi-junction cells considering atmospheric parameters fluctuation using Monte Carlo methods. In Proceedings of the PVSEC-27, Otsu, Japan, 12–17 November 2017.
31. Araki, K.; Ota, Y.; Sakai, T.; Lee, K.H.; Yamaguchi, M. Inherent uncertainty of energy ratings of multi-junction cells by the fluctuation of atmospheric parameters. In Proceedings of the PVSEC-27, Otsu, Japan, 12–17 November 2017.
32. Ota, Y.; Ueda, K.; Takamoto, T.; Nishioka, K. Output evaluation of a world's highest efficiency flat sub module with InGaP/GaAs/InGaAs inverted triple-junction solar cell under outdoor operation. Jpn. J. Appl. Phys. 2018, 57, 08RD08.
33. Itagaki, A.; Okumura, H.; Yamada, A. Preparation of meteorological data set throughout Japan for suitable design of PV systems Photovoltaic Energy Conversion. In Proceedings of the 3rd World Conference on Photovoltaic Energy Conversion, Osaka, Japan, 11–18 May 2003; Volume 2
34. Shirakawa K, Itagaki A, Utsunomiya T, 2011, Preparation of hourly solar radiation data on inclined surface (METPV-11) throughout Japan. In Proceedings of JSES/JWEA Joint Conference 2011, p. 193-196..

Preprints (www.preprints.org) | NOT PEER-REVIEWED | Posted: 2 January 2020 doi:10.20944/preprints202001.0018.v1

35. Nishimura A., Yasui T., Kitagawa S., Hirota M., Hu E. 2017, An Energy Supply Chain from Large Scale Photovoltaic Power Generation from Asian Cities to End Users in Japan, Smart Grid and Renewable Energy 8.05 (2017): 145.
36. Ota, Y.; Masuda, T.; Araki, K.; Yamaguchi, M. Curve-correction factor for characterization of the output of a three-dimensional curved photovoltaic module on a car roof. Coatings 2018, 8, 432.